ASTRONOMY & ASTROPHYSICS
SUPPLEMENT SERIES

Astron. Astrophys. Suppl. Ser. **112,** 143-149 (1995)

Optical properties of oxide dust grains

Th. Henning, B. Begemann, H. Mutschke and J. Dorschner

Max Planck Society, Research Group "Dust in Star-forming Regions", Schillergäßchen 2-3, D-07745 Jena, Germany

Received December 21, 1994; accepted February 4, 1995

Abstract. — In this paper, we present the optical properties of a series of well-characterized metal oxides ($Fe_xMg_{1-x}O$, x=1.0, 0.9, 0.8, 0.7, 0.5, 0.4) in the wavelength range from 200 nm to 500 μm. A number of oxygen-rich stars show circumstellar dust features between 10 and 14 μm and around 19 μm which cannot be explained by ordinary cosmic silicates but may be modelled by a mixture of aluminium oxide and iron-magnesium oxides. Calculated absorption spectra for small spheres show one vibrational band in the range from 19.9 μm (FeO) to 17.7 μm ($Fe_{0.4}Mg_{0.6}O$) in the Rayleigh limit. The absolute peak values of the oxide absorption bands are more than a factor of two larger than the 18 μm band of amorphous silicates, indicating that a small admixture of oxides can change the 18 μm/10 μm band ratio dramatically. The near-infrared opacity of the iron-rich oxides is of comparable magnitude to that of Fe_3O_4. Therefore, small amounts of iron-rich oxides in addition to silicates raise the absorbance in this spectral range in a very efficient way.

Key words: dust, extinction — infrared: stars; ISM: lines and bands — circumstellar matter — stars: AGB: post-AGB — methods: laboratory

1. Introduction

The composition of dust in circumstellar envelopes strongly depends on the O/C ratio, the pressure and temperature conditions, and the abundance of the most abundant elements forming refractory compounds. Assuming solar composition, these elements are iron, silicon, and magnesium (Anders & Grevesse 1989). However, we should note that Si, Fe, and Mg do not always show the same depletion pattern in the interstellar medium, pointing to grains with different Mg:Fe:Si ratios (e.g., Mathis 1993).

In an oxygen-rich environment around M-type stars, only basic constituents like MgO, SiO, FeO, atomic Fe and Mg are present in the gas phase prior to the formation of more complex silicate and oxide grains (Sedlmayr 1994; Nuth & Hecht 1990). The simultaneous observation of a 10 and 18 μm feature has generally been attributed to stretching and bending vibrations of Si–O bonds in cosmic silicates (for recent work see, e.g., Ossenkopf et al. 1992; Jäger et al. 1994). The appearance of a broad 12–13 μm feature in the LRS spectra of Mira variables with symmetric light curves is interpreted as due to aluminium oxide grains (e.g., Vardya et al. 1986; Onaka et al. 1989; Little-Marenin & Little 1990; Stencel et al. 1990). We should note that the formation of such aluminium oxide "stardust" is supported by the recent detection of presolar Al_2O_3 grains in the Bishunpur, Murchison, Orgueil, and Tieschitz meteorites (Hutcheon et al. 1994; Huss et al. 1994; Nittler et al. 1994).

Here, we stress that there are a number of oxygen-rich stars with IRAS LRS and UKIRT CGS 3 spectra showing some features between 10 and 14 μm which are very different from the classical silicate feature and that also show a feature at around 19 μm (see, e.g., Vardya et al. 1986; Little-Marenin & Little 1988, 1990; Groenewegen 1994). In the automatic classification of IRAS LRS spectra by Cheeseman et al. 1989, the spectra in the λ classes are dominated by emission bands at 11+, 13.1, and around 19 μm (see Goebel et al. 1989). Most of these IRAS sources are oxygen-rich stars. This may indicate that other metal oxides are present in the envelopes of these stars in addition to aluminium oxide and "normal" silicates. Good candidates for such metal oxides are iron-magnesium oxides with absorption in an interval around 19 μm (for a discussion of iron oxides, see also Duley 1980; Rietmeijer 1992). Such oxides could also contribute to the 18 μm feature in those cases where the feature is indeed due to stretching vibrations in silicates. This fact adds to the difficulty caused by the temperature distribution (see Henning et al. 1983) in attempts to derive an intrinsic 18 μm/10 μm silicate band strength from observed spectra. Recently, Goebel et al. (1994) detected a 7 μm feature in oxygen-rich shells, which lacks a clear identification. This shows again that spectra of these shells can be more complicated than would a "pure" silicate spectrum.

We extend the proposal by Nuth & Hecht (1990) who predicted the formation of a "chaotic" silicate and argued that the initial condensate will not be fully oxidized and that both aluminium and silicon will tend to reduce other metal oxides. Therefore, we would expect the presence of $Fe_xMg_{1-x}O$ grains with x between 0 and 1 in the envelopes of oxygen-rich stars.

To prove the presence of oxides in circumstellar and interstellar space, their optical properties have to be known and compared with observations. The optical constants of some of these refractory solids have already been determined. Here, we refer to the data for silicates (see, e.g., Jäger et al. 1994, pyroxene glass of cosmic composition; Dorschner et al. 1995, pyroxene and olivine glasses), Fe_2O_3 (Steyer 1974), Fe_3O_4 (Steyer 1974; Degiorgi et al. 1987), Al_2O_3 (Gervais 1991; Koike et al. 1995), MgO (Roessler & Huffman 1991),SiO (Philipp 1985a) and SiO_2 glass (Philipp 1985b). Data for FeO (wüstite) and its solid solution with MgO (periclase), called magnesiowüstite ($Fe_xMg_{1-x}O$) are not available yet. The main goal of this paper is to present such data for well-characterized samples of $Fe_xMg_{1-x}O$ from the ultraviolet to infrared wavelengths. Such laboratory data will be very important for an adequate interpretation of high-quality infrared observations expected to come from the Infrared Space Observatory ISO.

2. Oxide formation

The elements forming silicate and metal oxide grains are differently distributed in the gas and the grain phase in the interstellar medium. The depletions from the gas phase are not only dependent on the elements but also on the mean gas density (and of course on the age of the system) (Mathis 1993; Wilson & Rood 1994). These variations are not always well understood and sometimes point to the fact that the Solar System abundances may not be representative of the local ISM 4.6 Gyr ago.

However, the "cosmically" abundant elements O, Si, Mg, and Fe are expected to form refractory oxides (including highly-disturbed silicates) in oxygen-rich envelopes around evolved stars and supernovae shells (Nuth & Hecht 1990; Kozasa & Hasegawa 1989; Sedlmayr 1994). The formation of iron-magnesium oxides as well as additional metal oxides simultaneous with or independent of silicate formation or as a product of gas-grain reactions (in the diffuse interstellar medium) is possible under special conditions (Duley 1980; Jones 1990; Rietmeijer 1992). The understanding of the simultaneous formation of metal oxides and silicates is only possible by considering the nucleation process of silicates in detail (see Nuth & Hecht 1990; Stencel et al. 1990). One should note that Al (and SiO) are very efficient reducing agents and will balance the oxidation of Mg and Fe. In an oxygen-rich atmosphere, the non-equilibrium formation of iron-magnesium oxides can be expected. Assuming that oxide formation happens, the oxidation state of the excess iron in oxides, by that we mean the formation of FeO, Fe_3O_4, or Fe_2O_3, strongly depends on the prevalent oxygen partial pressure and the temperature regime. Decreasing temperature and increasing oxygen partial pressure shifts the equilibrium in the system Fe-Si-O from the formation of metallic iron to iron silicates, ferrous iron oxide (FeO, wüstite), mixed ferrous and ferric iron oxide (Fe_3O_4, magnetite), and completely oxidized ferric iron oxide (Fe_2O_3, hematite) (Frost 1991). The possibility that divalent iron can replace magnesium in the oxides and vice versa by the formation of solid solutions of $Fe_xMg_{1-x}O$ is due to the fact that the ionic radii of Fe^{2+} and Mg^{2+} are of comparable size.

Compared with the cosmic abundance value (0.5), the Fe/(Fe+Mg) ratio is different for interplanetary dust particles (IDPs) and comets. The dust of comet Halley shows a lower average value of 0.3 as measured by the mass spectrometers (Jessberger et al. 1989), indicating that the Halley silicate grains are magnesium-rich silicates. Examination of different chondritic IDPs (Christoffersen & Buseck 1986) show a great variety of Fe/(Fe+Mg) ratios; e.g., three olivine-dominated IDPs (members of the olivine IR class) show very different silicate compositions. JEDAI, a representative particle of this class, contains magnesium-rich olivine particles (Fe/(Fe+Mg) = 0.02), while the olivine grains in ESSEX and ATTILA are more Fe-rich particles (Fe/(Fe+Mg) = 0.28–0.61). In JEDAI, the Fe-components appear in the form of magnetite. In ESSEX and ATTILA, additional amounts of Fe-sulphides are described. This indicates that the occurrence of iron oxides together with magnesium silicates is not uncommon.

3. Preparation and chemical analysis

Bulk samples of FeO and $Fe_xMg_{1-x}O$ (x = 0.9, 0.8, 0.7, 0.5, 0.4) can be obtained by the quenching of melts. All preparational steps have to be performed under inert conditions to suppress the oxidation of ferrous (divalent) to ferric (trivalent) iron.

Stoichiometric mixtures of magnetite and metallic iron (or ferrous oxalate) with magnesium carbonate were pressed to pellets and melted in an arc furnace under argon. To avoid the disproportionation of ferrous iron during cooling, the melt droplets (0.5–1 cm diameter) were quickly quenched on a water cooled copper plate.

For the spectroscopic investigations as well as for electron microscopy (SEM with energy-dispersive X-ray analysis (EDX)) and X-ray diffraction studies, part of the dark bulk samples was embedded into an epoxide-resin and polished. The other part was used for the determination of the density. In addition, the ferrous iron content was determined by wet chemical analysis.

Global chemical analysis of bulk material by EDX points to an evaporative loss of iron during the melting

Table 1. Potentiometrical determination of the ferrous iron content (relative to the total iron content determined by means of EDX-analysis) of $Fe_xMg_{1-x}O$ samples (Cols. 2 to 3); Lattice constants (in picometres) of the samples (cubic, NaCl structure) compared with reference data (JCPDS database: FeO Nr. 6-615, MgO Nr. 4-829) (Cols. 4 & 5); Density of the samples measured after Archimedes' principle in CCl_4 in comparison with reference densities (Hammond 1991) (Cols. 6 & 7)

x	Fe total (EDX) (at.%)	ferrous iron content (at.%)	Lattice constant measured (pm)	Lattice constant Ref. data (pm)	Density measured (g/cm^{-3})	Density Ref. data (g/cm^{-3})
1.0	100	91	431	430.7	5.70	5.70
0.9	92	93			5.46	
0.8	79		429		5.25	
0.7	69	90	428		5.05	
0.4	42	99	426		4.79	
0.0	-	-		421.3	3.59	3.58

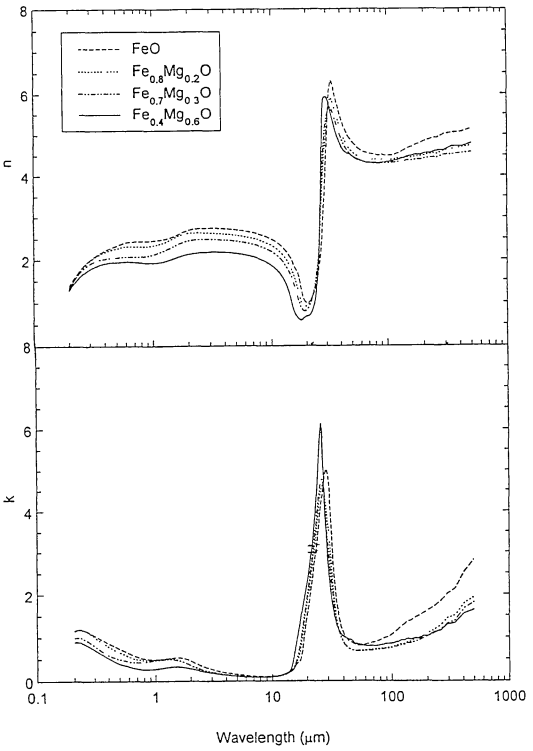

Fig. 1. Optical constants n and k for different iron-magnesium oxides in the wavelength region between 0.2 to 500 μm

process (for more details see Begemann et al. 1994). The knowledge of the ratio of ferrous to ferric iron is of great importance for the crystal structure and the interpretation of the IR spectra. FeO, $Fe_xMg_{1-x}O$ and MgO crystallize isotypically in the cubic NaCl structure. The iron and magnesium cations which are randomly distributed in the solid solutions $Fe_xMg_{1-x}O$ completely occupy the octahedral interstices in the cubic close packing of oxygen. The presence of ferric cations in $Fe_xMg_{1-x}O$ and in pure FeO leads to a non-stoichiometry of the compounds. The ferric cations are located in octahedral sites replacing ferrous iron and in normally unoccupied tetrahedral sites. The charge balance is provided by cation vacancies. The increase in the ferric iron content leads to the formation of magnetite instead of FeO. In pure magnetite, 1/3 of the total iron content is ferric iron. Its structure (inverse spinel) is based on a cubic close packing of oxygen similar to FeO. Half of the ferric iron is tetrahedrally surrounded by oxygen, the other half and the ferrous cations occupy the octahedral interstices in a statistical way.

An increase in the ferric iron content of the $Fe_xMg_{1-x}O$ samples changes the IR spectra dramatically. In addition to the 20 μm band due to octahedral vibrations of randomly distributed ferrous iron and magnesium cations, a band in the region around 18 μm appears. This band is comparable with the 17.5 μm band due to mixed tetrahedral and octahedral vibrations in pure magnetite. Such a feature was also observed in magnesiowüstite samples with an iron content smaller than 0.4. These samples could not be melted completely and were therefore not considered in this paper.

The ferrous iron content of our samples was determined potentiometrically by 0.05n CeIV-solution under inert conditions. This method is based on the redox reaction of ferrous iron with tetravalent cerium. As a first step, the bulk sample (no grinding) was disolved in hydrochloric acid (16 wt% HCl) at 323 K. After that, a 0.05n $Ce(NH_4)_2(SO_4)_3$ solution was added dropwise until the equivalence point, measured by means of two electrodes, was reached. The consumption of the CeIV-solution directly determines the ferrous iron content of the samples. $(NH_4)_2Fe(SO_4)_2 \times 6H_2O$ (Mohric salt) was measured as a ferrous iron standard. In Table 1, we show the ferrous iron content of our samples determined by this method.

The ferrous iron content of our FeO and $Fe_xMg_{1-x}O$ samples range between 90 and 99% of the total iron content. The small amounts of ferric iron left are too low to

Table 2. Optical constants of the wüstite and magnesiowüstite samples with the chemical compositions $Fe_xMg_{1-x}O$

	x=1.0		x=0.9		x=0.8		x=0.7		x=0.5		x=0.4	
λ (μm)	n	k	n	k	n	k	n	k	n	k	n	k
0.20	1.38	1.16	1.40	1.18	1.29	1.15	1.33	0.99	1.27	0.95	1.27	0.89
0.25	1.77	1.16	1.81	1.16	1.74	1.16	1.71	0.95	1.65	0.89	1.61	0.84
0.30	2.00	1.05	2.03	1.03	1.99	1.01	1.91	0.81	1.83	0.75	1.78	0.72
0.35	2.13	0.95	2.16	0.93	2.11	0.89	1.99	0.68	1.92	0.63	1.87	0.61
0.40	2.22	0.87	2.24	0.85	2.19	0.79	2.03	0.60	1.96	0.53	1.92	0.52
0.45	2.29	0.80	2.31	0.78	2.24	0.72	2.05	0.54	1.97	0.46	1.94	0.45
0.50	2.34	0.74	2.35	0.72	2.27	0.66	2.06	0.50	1.96	0.42	1.95	0.40
0.60	2.42	0.64	2.43	0.62	2.32	0.56	2.08	0.44	1.96	0.36	1.96	0.34
0.70	2.44	0.55	2.45	0.54	2.32	0.50	2.07	0.43	1.94	0.35	1.95	0.29
0.80	2.44	0.51	2.46	0.49	2.32	0.48	2.08	0.43	1.93	0.36	1.94	0.27
0.90	2.44	0.50	2.46	0.47	2.32	0.48	2.10	0.45	1.94	0.39	1.93	0.27
1.00	2.45	0.49	2.47	0.46	2.34	0.48	2.13	0.47	1.97	0.42	1.92	0.28
1.20	2.48	0.51	2.50	0.46	2.39	0.50	2.20	0.48	2.05	0.45	1.95	0.30
1.40	2.52	0.53	2.54	0.46	2.47	0.51	2.28	0.48	2.14	0.45	2.00	0.33
1.60	2.58	0.53	2.61	0.44	2.55	0.48	2.35	0.46	2.21	0.41	2.05	0.32
1.80	2.65	0.51	2.67	0.38	2.60	0.42	2.41	0.42	2.27	0.36	2.10	0.31
2.00	2.70	0.46	2.69	0.31	2.63	0.35	2.46	0.36	2.29	0.31	2.13	0.28
2.50	2.74	0.34	2.69	0.22	2.64	0.25	2.48	0.27	2.32	0.24	2.17	0.23
3.00	2.75	0.27	2.68	0.17	2.63	0.20	2.49	0.21	2.32	0.19	2.18	0.19
3.50	2.74	0.22	2.66	0.14	2.62	0.17	2.48	0.18	2.31	0.16	2.18	0.16
4.00	2.73	0.19	2.65	0.13	2.61	0.14	2.47	0.15	2.31	0.14	2.18	0.14
4.50	2.72	0.17	2.64	0.11	2.59	0.13	2.46	0.13	2.29	0.13	2.17	0.12
5.00	2.71	0.15	2.62	0.10	2.58	0.11	2.44	0.12	2.28	0.11	2.15	0.11
6.00	2.68	0.13	2.59	0.09	2.55	0.10	2.41	0.10	2.25	0.10	2.12	0.10
7.00	2.64	0.12	2.55	0.08	2.51	0.09	2.37	0.09	2.20	0.09	2.07	0.09
8.00	2.60	0.11	2.50	0.07	2.46	0.08	2.32	0.09	2.15	0.09	2.01	0.08
9.00	2.55	0.11	2.45	0.07	2.40	0.08	2.26	0.09	2.09	0.09	1.95	0.08
10.0	2.48	0.11	2.38	0.08	2.33	0.09	2.19	0.09	2.01	0.09	1.86	0.09
11.0	2.41	0.12	2.31	0.09	2.25	0.10	2.11	0.11	1.92	0.11	1.76	0.11
12.0	2.33	0.13	2.21	0.10	2.16	0.12	2.00	0.12	1.81	0.12	1.64	0.13
13.0	2.22	0.15	2.10	0.12	2.04	0.14	1.88	0.15	1.68	0.15	1.48	0.17
14.0	2.10	0.19	1.97	0.15	1.90	0.19	1.73	0.20	1.50	0.20	1.26	0.23
15.0	1.94	0.24	1.80	0.20	1.72	0.25	1.53	0.28	1.24	0.31	0.93	0.41
16.0	1.79	0.36	1.60	0.30	1.51	0.36	1.30	0.42	1.03	0.57	0.73	0.78
17.0	1.63	0.42	1.37	0.38	1.25	0.56	1.05	0.68	0.86	0.87	0.63	1.15
18.0	1.29	0.60	1.02	0.68	1.01	0.90	0.87	1.06	0.74	1.24	0.59	1.55
19.0	1.06	1.02	0.87	1.14	0.91	1.33	0.81	1.49	0.71	1.64	0.65	1.90
20.0	0.99	1.46	0.84	1.56	0.91	1.75	0.83	1.92	0.75	2.05	0.68	2.23
21.0	1.01	1.88	0.87	1.99	0.98	2.17	0.91	2.34	0.83	2.46	0.70	2.63
22.0	1.08	2.29	0.95	2.40	1.10	2.58	1.03	2.77	0.96	2.91	0.78	3.09
23.0	1.20	2.69	1.07	2.82	1.27	3.03	1.23	3.25	1.18	3.40	0.92	3.63
24.0	1.36	3.11	1.25	3.27	1.53	3.51	1.56	3.76	1.53	3.91	1.18	4.30
25.0	1.61	3.56	1.53	3.75	1.95	3.98	2.06	4.26	2.06	4.45	1.72	5.11
26.0	1.95	4.00	1.91	4.23	2.54	4.40	2.81	4.66	2.90	4.91	2.85	5.90
27.0	2.42	4.42	2.50	4.71	3.33	4.62	3.78	4.76	4.13	4.93	4.83	5.89
28.0	3.05	4.79	3.30	4.99	4.17	4.50	4.66	4.39	5.06	4.20	5.84	4.48
29.0	3.86	5.01	4.16	5.00	4.81	4.15	5.20	3.80	5.37	3.42	5.92	3.51
30.0	4.82	4.92	5.00	4.79	5.27	3.73	5.47	3.26	5.45	2.85	5.93	2.85
31.0	5.69	4.43	5.77	4.35	5.64	3.28	5.64	2.79	5.45	2.41	5.82	2.34
32.0	6.18	3.64	6.34	3.60	5.85	2.75	5.68	2.34	5.40	2.06	5.65	1.94
33.0	6.32	2.88	6.48	2.78	5.90	2.25	5.65	1.97	5.32	1.79	5.48	1.68
34.0	6.22	2.35	6.37	2.18	5.80	1.86	5.55	1.66	5.22	1.56	5.33	1.49
35.0	6.08	1.96	6.18	1.76	5.68	1.57	5.43	1.44	5.12	1.40	5.20	1.35
36.0	5.90	1.68	5.98	1.47	5.54	1.35	5.32	1.26	5.03	1.27	5.06	1.23
38.0	5.66	1.33	5.66	1.11	5.31	1.06	5.11	1.02	4.86	1.07	4.89	1.11

Table 3. continued

	x=1.0		x=0.9		x=0.8		x=0.7		x=0.5		x=0.4	
λ (μm)	n	k	n	k	n	k	n	k	n	k	n	k
40.0	5.41	1.13	5.38	0.91	5.11	0.90	4.94	0.89	4.72	0.96	4.74	1.03
42.0	5.22	0.99	5.18	0.79	4.94	0.80	4.80	0.80	4.61	0.89	4.64	0.98
44.0	5.10	0.92	5.02	0.73	4.82	0.74	4.70	0.75	4.53	0.85	4.58	0.96
46.0	4.97	0.88	4.92	0.69	4.72	0.72	4.61	0.71	4.48	0.81	4.54	0.94
48.0	4.91	0.85	4.82	0.67	4.65	0.70	4.54	0.69	4.42	0.78	4.53	0.90
50.0	4.83	0.82	4.75	0.66	4.59	0.68	4.48	0.68	4.37	0.76	4.48	0.84
60.0	4.62	0.83	4.56	0.64	4.44	0.69	4.35	0.68	4.27	0.74	4.37	0.79
70.0	4.54	0.87	4.50	0.66	4.40	0.71	4.30	0.69	4.25	0.76	4.32	0.80
80.0	4.51	0.93	4.47	0.68	4.39	0.73	4.30	0.72	4.26	0.76	4.30	0.81
90.0	4.52	0.99	4.44	0.70	4.40	0.75	4.30	0.74	4.29	0.77	4.33	0.85
100	4.49	1.06	4.44	0.72	4.39	0.77	4.30	0.75	4.31	0.77	4.34	0.86
120	4.54	1.24	4.44	0.80	4.42	0.85	4.33	0.82	4.34	0.78	4.38	0.93
140	4.64	1.38	4.46	0.87	4.43	0.90	4.36	0.87	4.37	0.79	4.45	0.96
160	4.72	1.46	4.47	0.93	4.45	0.96	4.38	0.91	4.38	0.81	4.49	0.98
180	4.79	1.54	4.49	0.99	4.47	1.02	4.39	0.96	4.39	0.84	4.51	1.00
200	4.85	1.62	4.50	1.07	4.50	1.09	4.42	1.02	4.41	0.86	4.55	1.03
250	4.93	1.81	4.54	1.25	4.53	1.25	4.45	1.16	4.46	0.96	4.61	1.14
300	5.02	2.03	4.63	1.43	4.62	1.45	4.52	1.33	4.48	1.11	4.65	1.30
350	5.05	2.18	4.62	1.53	4.66	1.54	4.53	1.42	4.54	1.14	4.72	1.36
400	5.06	2.48	4.64	1.75	4.69	1.75	4.55	1.63	4.52	1.30	4.72	1.52
450	5.10	2.66	4.63	1.88	4.71	1.86	4.56	1.74	4.54	1.33	4.76	1.59
500	5.15	2.82	4.62	2.00	4.74	1.94	4.58	1.82	4.57	1.34	4.80	1.63

significantly affect the infrared spectra and X-ray diffraction measurements.

The lattice constants of the FeO and $Fe_xMg_{1-x}O$ samples could not be determined very accurately from the X-ray diffraction measurements because the high degree of lattice disorder leads to strongly broadened Bragg reflexes. Nevertheless, the tendency of decreasing cell dimensions of the cubic FeO lattice with increasing magnesium content (see Table 1) could be distinguished in our dataset.

The density of the bulk samples of $Fe_xMg_{1-x}O$ (Table 1) was measured in CCl_4 after Archimedes' principle. Our measurements of FeO and MgO are in good agreement with the reference data. With increasing magnesium content, the density of the mixed crystals decreases.

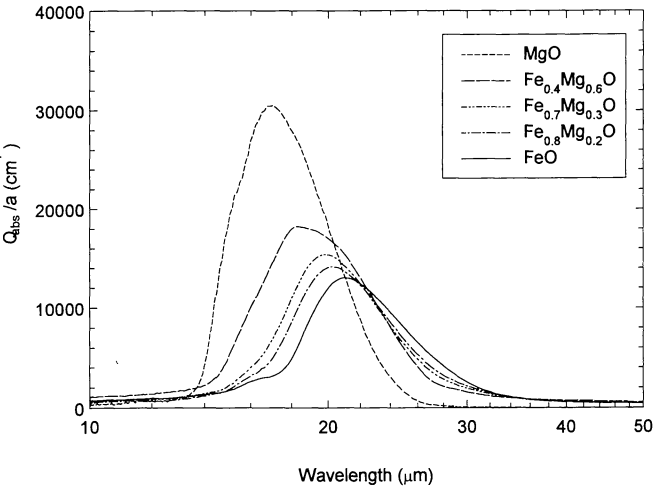

Fig. 2. Absorption efficiencies normalized to an effective radius for the different iron-magnesium oxides computed for the CDE with the quadratic weighting function (see text)

4. Spectroscopic results

The specular reflectance at near normal incidence of the polished sample surfaces has been measured in the wavelength range from 0.2 to 500 μm using a Perkin Elmer Lambda 19 UV/VIS/NIR instrument and a Bruker 113v FTIR spectrometer. A calibrated aluminium mirror was used as a reference sample.

The complex refractive index $n + ik$ of the materials has been determined by a combination of a Lorentz oscillator fit method (typically 5 oscillators) in the region from the ultraviolet to mid-infrared wavelengths with Kramers-Kronig analysis in the region of the infrared vibrational bands. For the latter method, the reflectance, R, was extrapolated to infinite wavelengths assuming an approach to unity. At the short wavelength side, the criterion $\int_{-\infty}^{\infty} \ln(R(\omega)/R(\infty))d\omega = 0$ required by causality (Harbecke 1986) was used to ensure that a physically correct extrapolation was chosen. Here, the quantity ω is the wavenumber. The optical constants obtained by the two

methods show excellent agreement in the overlap region between 5 and 10 μm.

The resulting optical constants are given in Fig. 1 and Table 2. They are dominated by an infrared vibrational band with a maximum in k at about 25 μm that is shifted to shorter wavelengths with growing Mg content. In the very far IR (λ >100 μm) the absorption index, k, increases again. This is due to a Drude-like behaviour caused by the presence of free charge carriers in the semiconducting materials.

In the near infrared and at shorter wavelengths, the optical behaviour is mainly determined by the electronic structure of the iron ions. Here, two very broad bands at about 0.23 and 1.5 μm have been observed. The band positions show some similarity to bands observed in magnetite (Fe_3O_4) (Schlegel et al. 1979) and also in olivine (Burns 1970; Dorschner et al. 1995). This is due to similar environments of the iron ions (Fe^{2+} in octahedral coordination and Fe^{3+} in octahedral and tetrahedral coordination) in these materials.

For a comparison with astronomical data, the absorption behaviour of materials with these optical constants is interesting. It is a well-known fact (see Bohren & Huffman 1983) that spheres composed of materials with strong absorption bands have strong and narrow resonances which are washed out in a size/shape distribution of particles. Therefore, we calculated absorption efficiencies for small particles of spherical and ellipsoidal shapes in the Rayleigh limit. For ellipsoidal grains, we used the formulae for a continuous distribution of ellipsoids (CDE) given by Bohren & Huffman (1983) and for a CDE with a quadratic weighting function having its maximum for the sphere as used by Ossenkopf et al. (1992). The infrared band positions determined by these calculations are summarized in Table 3. For the weighted CDE which in our opinion is the best approximation to a real particle shape distribution, the calculated absorption efficiencies in the band region, normalized to the radius of spheres of identical volume, are given in Fig. 2. In the visible range, the normalized absorption efficiencies reach values of 5E4-1E5 cm^{-1} increasing with increasing iron content. In the FIR, the absorption efficiency decreases proportional to $\lambda^{-0.7}$ ($\lambda^{-0.9}$ for spheres). Here we should note that all calculations were done in the Rayleigh limit. In this case, the quantity Q_{abs}/a is independent of the grain size.

Compared with the 18 μm band of amorphous silicates, the absolute peak values of the oxide absorption bands (weighted CDE) are larger by a factor of 2 for FeO and up to a factor of 4.5 for MgO. Therefore, a small admixture of oxides can dramatically change the absorption spectrum of silicates, especially the 18 μm/10 μm band ratio considerably (see also Nuth & Hecht 1990). To illustrate this fact, we calculated absorption spectra caused by a mixture of separate oxide and pyroxene glass grains (data for the latter materials are taken from Dorschner et al. 1995). Here, we present the very interesting extreme cases in which iron is considered to be present either only in the oxide or only in the silicate phase (Fig. 3). A small quantity of FeO or MgO broadens the 18 μm band, whereas for higher proportions, the oxide absorption clearly dominates and shifts the band to longer wavelengths in the case of FeO and towards shorter wavelengths for MgO.

Table 4. Positions of the infrared bands for $Fe_xMg_{1-x}O$ calculated from the optical data of Table 2 for different particle shapes

x	Spheres	Weighted CDE (Ossenkopf et al. 1992)	CDE (Bohren & Huffman 1983)
1.0	19.9	21.0	23.4
0.9	19.6	20.7	22.9
0.8	19.2	20.2	22.4
0.7	18.8	19.9	21.9
0.5	18.5	19.4	21.5
0.4	17.7	18.3	21.4
0.0	16.3	17.0	19.0

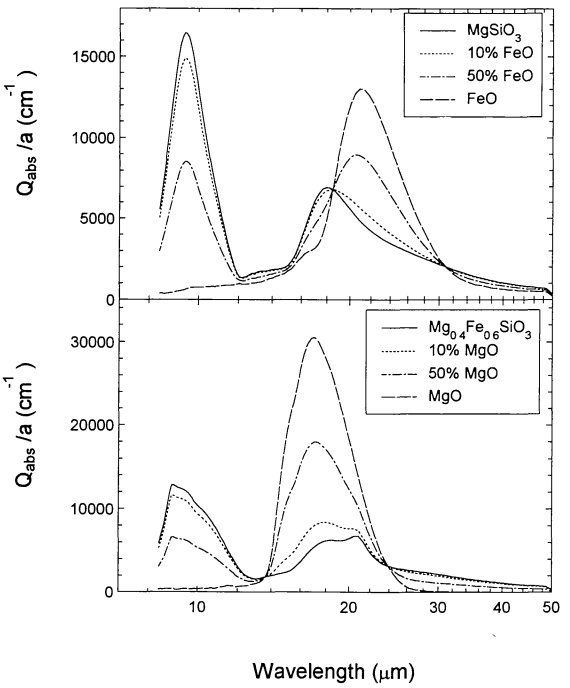

Fig. 3. Absorption efficiencies normalized to an effective radius for mixtures of glassy $MgSiO_3$ with different percentages of FeO (upper part) and mixtures of glassy $Mg_{0.4}Fe_{0.6}SiO_3$ with MgO (lower part) computed for the CDE with the quadratic weighting function (see text). For the sake of comparison, the curves for pure FeO and MgO are also shown

5. Conclusions

In this paper, we present new optical data for iron-magnesium oxides ($Fe_xMg_{1-x}O$ x=1.0, 0.9, 0.8, 0.7, 0.5, 0.4) from 200 nm to 500 μm. The data were obtained from reflection measurements of well characterized (composition, ferrous iron content, crystallinity, density) samples. Calculated absorption spectra for small spheres in the Rayleigh limit, for the CDE and weighted CDE show a shifting of the vibrational band towards shorter wavelengths with increasing magnesium content. For small spheres, the peak values are located in the wavelength range between 19.9 μm (FeO) and 17.7 μm ($Fe_{0.4}Mg_{0.6}O$). Calculations for the CDE and weighted CDE indicate a broadening of the band and a shifting of the peak's wavelength towards larger values (FeO: weighted CDE: 21.0 μm, CDE: 23.4 μm; $Fe_{0.4}Mg_{0.6}O$: weighted CDE: 18.3 μm, CDE: 21.4 μm). This vibrational band of metal oxides can considerably contribute to or even completely dominate the observed 18–19 μm feature in some oxygen-rich stars. The presence of iron-rich oxides in addition to magnesium-rich silicates will shift the 18 μm band produced by the silicates towards longer wavelengths. The "addition" of oxides will also increase the intensity of the 18 μm band. This may change the 18 μm/10 μm band ratio dramatically. In oxygen-rich sources without classical 10 and 18 μm silicate bands (λ-classes in the IRAS-LRS catalogue), the broad 19 μm feature can easily be explained by iron-magnesium oxides. The near-infrared opacity of the iron-rich oxides is of comparable magnitude to that of Fe_3O_4 and Fe_2O_3. Therefore, the presence of iron-rich oxides can strongly increase the dust absorbance in the near-infrared spectral region. The data given in this paper should be extremely useful for the interpretation of the high-quality data expected to come from the Infrared Space Observatory.

References

Anders E., Grevesse N. 1989, Geochim. Cosmochim. Acta 53, 197

Begemann B., Henning Th., Mutschke H., Dorschner J. 1994, Planet. Space Sci., in press

Bohren C.F., Huffman D.R. 1983, Absorption and Scattering of Light by Small Particles (John Wiley & Sons, New York)

Burns R.B. 1970, Mineralogical Applications of Crystal Field Theory (Cambridge University Press, London)

Cheeseman P., Stutz J., Self M. et al. 1989, Automatic Classification of Spectra from the Infrared Astronomical Satellite (IRAS), NASA Reference Publ., 1217

Christoffersen R., Buseck P.R. 1986, Earth Planet. Sci. L78, 53

Degiorgi L., Blatter-Mörke I., Wachter P. 1987, Phys. Rev. B 35, 5421

Dorschner J., Begemann B., Henning Th., Jäger C., Mutschke H. 1995, A&A, in press

Duley W.W. 1980, ApJ 240, 950

Frost B.R. 1991, ed. D.H. Lindsley, Oxide Minerals: Petrologic and Magnetic Significance, Min. Soc. America 25, 1

Gervais F. 1991, ed. E.D. Palik, Handbook of Optical Constants of Solids II (Academic Press, Boston) 761

Goebel J., Volk K., Walker H. et al. 1989, A&A 222, L5

Goebel J.H., Bregman J.D., Witteborn F.C. 1994, ApJ 430, 317

Groenewegen M.A.T. 1994, A&A 290, 207

Harbecke B. 1986, Appl. Phys. A 40, 151

Hammond C.R. 1991, ed. D.R. Lide, CRC Handbook of Chemistry and Physics (CRC Press, Boca Raton) 4, p. 1

Henning Th., Gürtler J., Dorschner J. 1983, Ap&SS 94, 333

Huss G.R., Fahey A.J., Gallino R., Wasserburg G.J. 1994, ApJ 430, L81

Hutcheon I.D., Huss G.R., Fahey A.J., Wasserburg G.J. 1994, ApJ 425, L97

Jäger C., Mutschke H., Begemann B., Dorschner J., Henning Th. 1994, A&A 292, 641

Jessberger E.K., Kissel J., Rahe J. 1989, eds. S.K. Atreya, J.B. Pollack, M.S. Matthews, Origin and Evolution of Planetary and Satellite Atmospheres (Univ. Arizona Press, Tucson) 167

Jones A.P. 1990, MNRAS 245, 331

Koike C., Kaito C., Yamamoto T., Shibai H., Kimura S., Suto H. 1995, submitted

Kozasa T., Hasegawa H. 1989, ApJ 344, 325

Little-Marenin I.R., Little S.J. 1988, ApJ 333, 305

Little-Marenin I.R., Little S.J. 1990, AJ 99, 1173

Mathis J.S. 1993, Reports Progr. Phys. 56, 605

Nittler L.R., O'D Alexander C.M., Gao X., Walker R.M., Zinner E.K. 1994, Nature 370, 443

Nuth III J.A., Hecht J.H. 1990, Ap&SS 163, 79

Onaka T., de Jong T., Willems F.J. 1989, A&A 218, 169

Ossenkopf V., Henning Th., Mathis J.S. 1992, A&A 261, 567

Philipp H.R. 1985a, ed. E.D. Palik, Handbook of Optical Constants of Solids (Academic Press, Boston) 765

Philipp H.R. 1985b, ed. E.D. Palik, Handbook of Optical Constants of Solids (Academic Press, Boston) 749

Rietmeijer F.J.M. 1992, ApJ 400, L39

Roessler D.M., Huffman D.R. 1991, ed. E.D. Palik, Handbook of Optical Constants of Solids II (Academic Press, Boston) 919

Schlegel A., Alvarado S.F., Wachter P. 1979, J. Phys. C 12, 1157

Sedlmayr E. 1994, ed. U.G. Jørgensen, Molecules in the Stellar Environment (Springer Verlag, Berlin) 163

Stencel R.E., Nuth III J.A., Little-Marenin I.R. 1990, ApJ 350, L45

Steyer T.R. 1974, Ph.D. thesis, University of Arizona

Vardya M.S., de Jong T., Willems F.J. 1986, ApJ 304, L29

Wilson T.L., Rood R.T. 1994, ARA&A 32, 191